Structural and Kinetic Analyses Reveal the Dual Inhibition Modes of Ornithine Aminotransferase by (1*S*,3*S*)-3-Amino-4-(Hexafluoropropan-2-Ylidenyl)-Cyclopentane-1-Carboxylic Acid (BCF_3)

Arseniy Butrin[1], Brett A. Beaupre[1], Noel Kadamandla[1], Peidong Zhao[1], Sida Shen[2], Richard B. Silverman[2,3], Graham R. Moran[1], and Dali Liu[1,*]

[1] Department of Chemistry and Biochemistry, 1068 W Sheridan Rd, Loyola University Chicago, Chicago, IL 60660.

[2] Department of Chemistry, Chemistry of Life Processes Institute, Center for Molecular Innovation and Drug Discovery, Center for Developmental Therapeutics, Northwestern University, 2145 Sheridan Rd, Evanston, IL 60208

[3] Department of Molecular Biosciences, Northwestern University, Evanston, IL 60208; Department of Pharmacology, Feinberg School of Medicine, Northwestern University, Chicago, IL 60611

*Corresponding author; phone: (773)508-3093; email: dliu@luc.edu

Abstract

Hepatocellular carcinoma (HCC) is the most common form of liver cancer and the leading cause of death among people with cirrhosis. HCC is typically diagnosed in advanced stages when tumors are resistant to both radio- and chemotherapy. Human ornithine aminotransferase (*h*OAT) is a pyridoxal-5′-phosphate (PLP)-dependent enzyme involved in glutamine and proline metabolism. Because *h*OAT is overexpressed in HCC cells and a contributing factor for the uncontrolled cellular division that propagates malignant tumors (Ueno, A. *et al.*, *J. Hepatol.* **2014**, *61*, 1080-1087), it is a potential drug target for the treatment of HCC. (1*S*,3*S*)-3-Amino-4-(hexafluoropropan-2-ylidenyl)-cyclopentane-1-carboxylic acid (BCF_3) has been shown in animal models to slow the progression of HCC by acting as a selective and potent mechanism-based inactivator of OAT (Zigmond *et al*., *ACS Med. Chem. Lett.* **2015**, 6, 8, 840–844). Previous studies have shown that the BCF_3-*h*OAT reaction has a bifurcation in which only 8% of the inhibitor inactivates the enzyme while the remaining 92% ultimately acts as a substrate and undergoes hydrolysis to regenerate the active PLP form of the enzyme. In this manuscript, the rate-limiting step of the inactivation mechanism was determined by stopped-flow spectrophotometry and time-dependent ^{19}F-NMR experiments to be the decay of a long-lived external aldimine species. A crystal structure of this transient complex revealed both the structural basis for fractional irreversible inhibition and the principal mode of inhibition of *h*OAT by BCF_3, which is to trap the enzyme in this transient but quasi-stable external aldimine form.

Introduction

Aminotransferases represent a group of PLP-dependent enzymes that use a "Bi-Bi, Ping-Pong" mechanism to catalyze the transfer of an amino group, typically donated by an amino acid to an acceptor α-keto acid[1-3]. In the first half-reaction, an amino acid is oxidized with the concomitant reduction of the PLP coenzyme to pyridoxamine-5'-phosphate (PMP). In the second half-reaction, the amino group from PMP is transferred to a suitable α-keto acid acceptor with the concomitant oxidation of PMP to regenerate the PLP coenzyme. The transamination mechanism of *h*OAT exhibits these two canonical half-reactions with the conversion of L-ornithine and PLP to glutamate-γ-semialdehyde and PMP followed by the conversion of α-ketoglutarate and PMP to L-glutamate and PLP (**Scheme 1**).

Scheme 1. The Chemistry of OAT

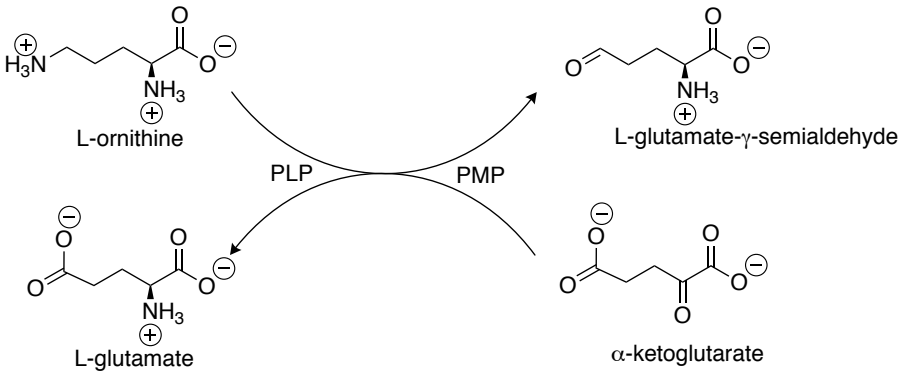

*h*OAT in mammals is transported into the mitochondrial matrix and is in high abundance in the brain, intestines, kidneys, and liver. It functions at a nexus for multiple metabolic pathways including glutamine metabolism, proline synthesis, and the urea cycle[4]. Knockout experiments of the *oat* gene revealed that OAT may not have an important role in mitosis within normally developing cells[4]. However, studies by Wang et al. have implicated *h*OAT in the assembly of the

mitotic spindle in human cancer cells[5]. Complex coordination of the components of the mitotic spindle is essential for successful separation of the sister chromatids. Moreover, inhibition of OAT is expected to diminish cellular glutamate and proline, both of which are important metabolites in neoplastic cells. Therefore, inhibition of *h*OAT is one path to slow cell division in cancer cells.

Mehta et al.[2] performed a sequence alignment of 14 aminotransferases, including GABA aminotransferase (GABA-AT), L-aspartate aminotransferase (Asp-AT), and *h*OAT, and found that while they share low sequence identity, the available structures indicate highly similar tertiary folds[4-6]. The highly conserved residues in the active sites of different aminotransferases make it difficult to selectively inhibit one enzyme without generating off-target reactivity and associated toxicity. Known irreversible inhibitors for both OAT and GABA-AT, such as gabaculine and 4-amino-5-hexynoic acid lack desired selectivity[6]. Although active site residues may be conserved, aspects of the chemical mechanism of each enzyme are unique. Therefore, the key to the rational design of a selective inactivator of an aminotransferase is based on an understanding of the specific chemistry involved.

Scheme 2. Proposed Inactivation Mechanism of *h*OAT by BCF_3

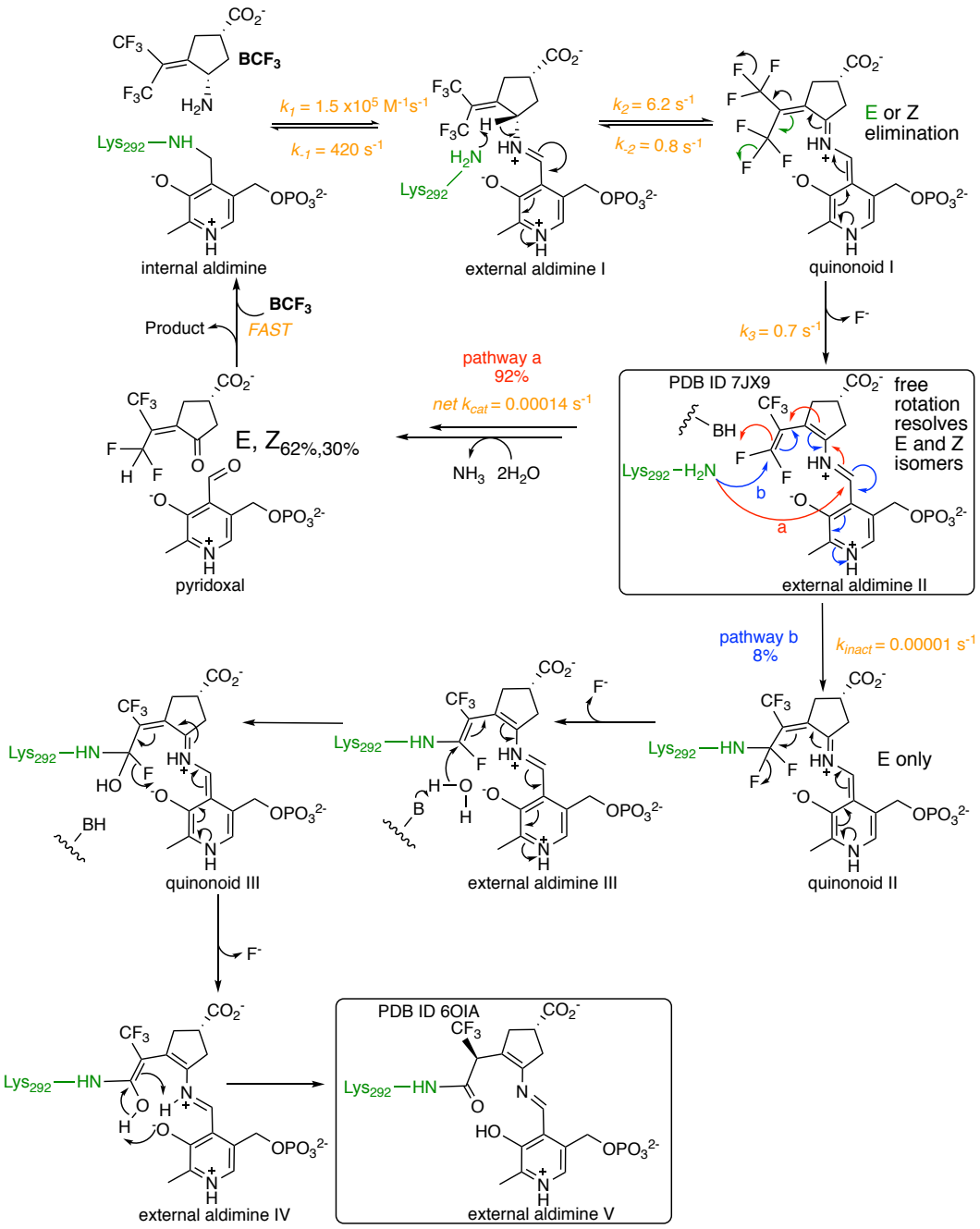

(1*S*,3*S*)-3-Amino-4-(hexafluoropropan-2-ylidenyl)-cyclopentane-1-carboxylic acid (named here as BCF_3 after the (Bis)trifluoromethyl feature) is an irreversible inhibitor of *h*OAT

that showed promising results for suppression of HCC tumor growth in athymic mice implanted with human-derived HCC[7]. BCF_3 covalently and irreversibly modifies both the catalytic lysine 292 and PLP, forming a tethered tertiary adduct that inactivates the enzyme. The currently proposed inactivation mechanism of BCF_3 lacks experimental proof for the proposed intermediate complexes, and the rate-limiting step was hitherto yet to be identified[8]. To better understand the nature of *h*OAT as a drug target and facilitate the rational design of agents active against HCC, it is essential to quantitatively establish and verify the mechanism of BCF_3 inhibition. This work presents an investigation of *h*OAT inactivation by BCF_3 using a combined approach of transient-state kinetics and X-ray crystallography. The conclusions we have drawn incorporating the data from these additional methodologies are summarized in (**Scheme 2)**.

RESULTS AND DISCUSSION

Mechanism-based inactivators commandeer the chemical mechanism of an enzyme to covalently and irreparably alter functional groups in the active site[9]. The rational design of covalent inactivators based on a detailed understanding of the chemical mechanism has great potential for drug discovery, as such an approach builds in both potency and specificity simultaneously. Methods to verify the chemistry of such inactivators most often include inhibition assays, mass spectrometry and X-ray crystallography[10-14]. Although these approaches have been successful in describing the inactivation mechanisms of PLP-dependent enzymes, the amenability of such enzymes to transient-state approaches allows for more comprehensive evaluation, particularly those that exhibit multiple intermediates and partitions.

PLP-dependent transaminase reactions are often studied by spectrophotometric transient-state measurements as they exhibit predictable sequences of spectrophotometrically identifiable intermediates with absorption transitions from 300-650 nm[15-17]. However, the identity of new intermediates or reaction endpoints cannot be based solely on absorption spectra. For such species, it is necessary to employ complementary approaches in parallel to define the chemistry that is occurring. The kinetics of the BCF_3 inhibition of *h*OAT has rates that span seven orders of magnitude (**Scheme 2**) and can be studied by spectroscopic methods that have fast and slow integration times. Here we employ rapid mixing spectrophotometric, time-dependent NMR, and steady-state X-ray crystallography/crystal-soaking methods to reveal the detailed inhibition mechanism of *h*OAT reacting with BCF_3.

Transient State Measurements of *h*OAT Inactivation by BCF_3: A combination of spectrophotometric and NMR measurements was used to capture the kinetics of the inhibition of

*h*OAT by BCF_3. This inhibition process had previously been characterized by mass spectroscopy and X-ray crystallography[8]. The approaches used take advantage of the highly conjugated species that occur sequentially, the unique NMR shifts of ^{19}F correlated with additional X-ray structural data (see below). These measurements provide a more complete assignment of the inactivation chemistry of *h*OAT by BCF_3. Titration of *h*OAT with BCF_3 modulated the rate of accumulation of a quinonoid intermediate observed maximally at 567 nm (**Figure 1**).

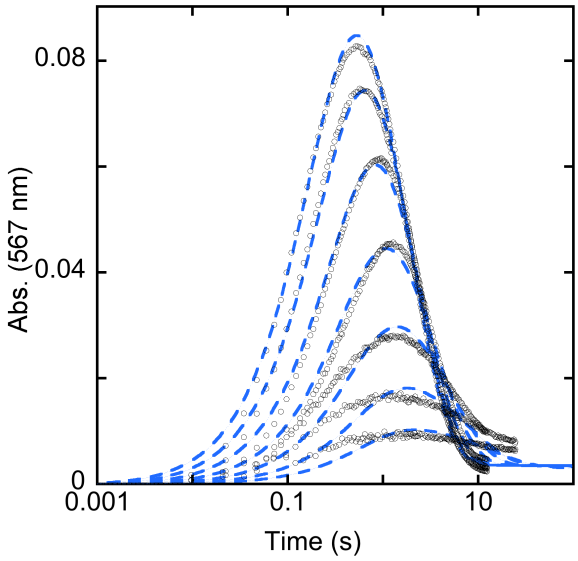

Figure 1. Transient state absorption changes observed at 567 nm for *h*OAT reacting with BCF_3. *h*OAT (9.84 μM) was allowed to react with BCF_3 (63, 127, 254, 508, 1016, 2035, 4065 μM) and CCD spectra were collected on two timeframes (0.009-12.3 seconds for concentrations 63, 127, 254 μM, and 0.02 – 24 sec for concentrations 508, 1016, 2035, 4065 μM). The extracted 576 nm data were fit to a linear model shown in orange in **Scheme 3** and returned the rate constants shown in **Scheme 2**.

The formation and decay of this intermediate could be fit to a reversible three-step model shown in orange in **Scheme 3** and the rate constants returned from the fit are shown in **Scheme 2**. The observed rate of formation of the quinonoid is a function of the extent of population and rate of decay of the preceding external aldimine species (see below). As such these data report both on

the individual rate constants for formation and decay of three species and the prior equilibrium for formation of the initial external aldimine. The global fit gave rate constants of $k_1 = 1.5\text{x}10^5 \pm 3\text{x}10^4$ $M^{-1}s^{-1}$, $k_{-1} = 421 \pm 64$ s^{-1} for formation of the external aldimine I (**Scheme 2**). The dissociation constant for the reversible formation of this species was therefore 3.0 ± 0.5 mM. The subsequent formation of the quinonoid species was described by rate constants $k_2 = 6.18 \pm 0.24$ s^{-1} and $k_{-2} = 0.81 \pm 0.02$ s^{-1}. The irreversible decay of the quinonoid was fit to yield a rate constant of $k_3 = 0.74 \pm 0.01$ s^{-1}.

Scheme 3. Four step model for the intermediates observed via CCD 340-700 nm and ^{19}F-NMR spectrometry. The first three reaction steps (orange box) were observed for a range of BCF_3 concentrations and analyzed globally by numerical integration at a single wavelength (567 nm). The rate constants associated with the second and third steps (green box) were derived from CCD data using singular value decomposition (SVD). The data for the last step (blue box) were acquired with ^{19}F-NMR spectrometry and analyzed using SVD.

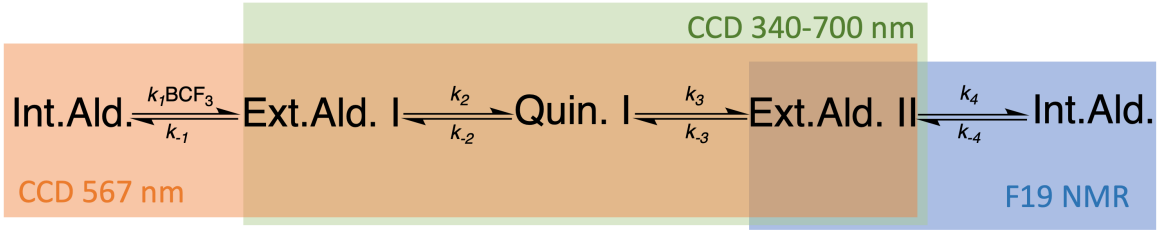

Three-dimensional CCD data recorded for a single concentration of BCF_3 (**Figure 2A**) were fit globally using SVD to deconvolute and define pure spectra of the intermediates observed (**Figure 2B**). These data were fit to a simplified three-step irreversible model and thus did not return evidence of reversibility. The rate constants obtained from the fit agree well with those determined from the single wavelength analysis at 567 nm ($k_2 = 5.13 \pm 0.03$ s^{-1} and $k_3 = 0.51 \pm 0.01$ s^{-1}).

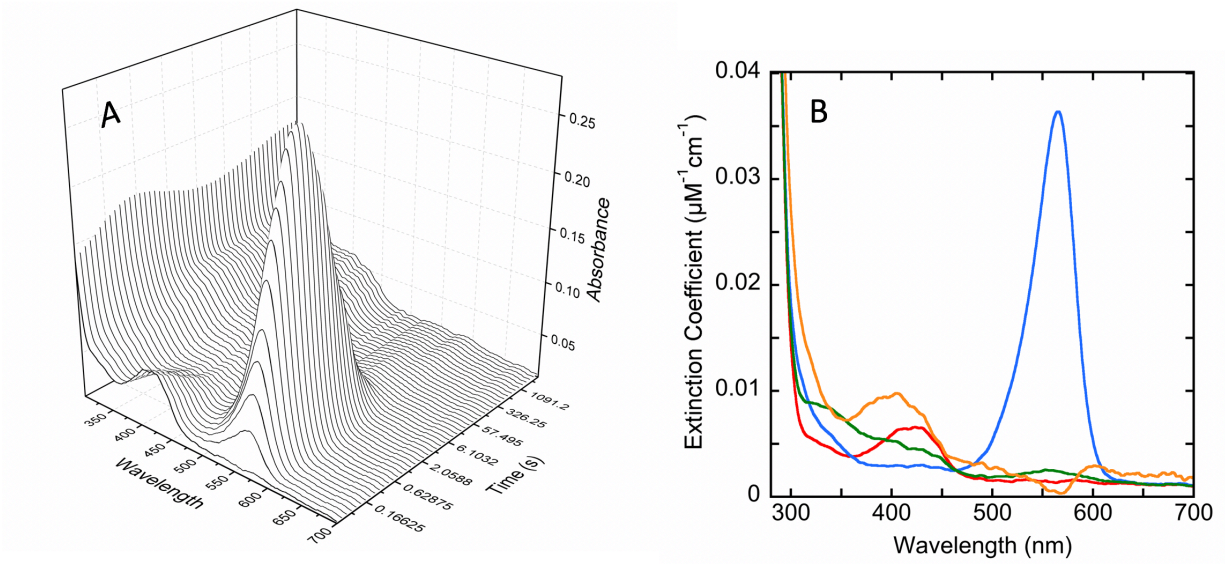

Figure 2. Transient-state CCD data for *h*OAT reacting with BCF_3. A. *h*OAT (9.84 μM final) was mixed with BCF_3 (4065 μM) and CCD spectra were collected on two timeframes (0.0025 – 12.5, 15-2500 sec) and spliced together at ~12 sec to form a single data set for analysis. The data were fit using the SVD routine available in KinTek Explorer software to a linear model shown in green in **Scheme 3**, where the last rate constant was fixed to that determined from the time-dependent NMR data shown in **Figure 3** and returned rate constants shown in **Scheme 2**. B. Spectra shown are the deconvoluted spectra assigned as follows: red; external aldimine I, blue; quinonoid I, green; external aldimine II, and orange; pyridoxal 5'-phosphate.

As described above, the final step k_4 was fixed to the value measured by transient state ^{19}F-NMR spectrometry. Time-dependent ^{19}F-NMR signals were fit using the SVD module of KinTeK Explorer software (**Figure 3**) and returned a rate constant of 0.00015 ± 0.00003 s^{-1}. This value is a net rate that describes a bifurcation and includes events for the decay of the external aldimine II species that liberates PLP (**Scheme 2**) and the rate of formation of the covalently modified *h*OAT. Prior data indicated that in any one turnover, 92% of the reaction yields PLP[8]; as such, the two rate constants diverging from the bifurcating step are summed from this rate and are k_{cat} = 0.00014 s^{-1} and k_{inact} = 0.00001 s^{-1}. These values describe the rates for substrate and inhibitor roles of BCF_3, respectively. The dominant path for decay of external aldimine II reinstates the PLP form of the cofactor permitting subsequent turnovers with BCF_3. This net rate constant is four orders of

magnitude slower than any other step which dictates that the BCF_3 turnover rate is defined by this value (k_{cat}). That no other spectrophotometrically conspicuous species, such as a subsequent quinonoid state, are observed suggests that the measured k_{inact} can be ascribed specifically to the first step in the inhibitory path for decay of external aldimine II.

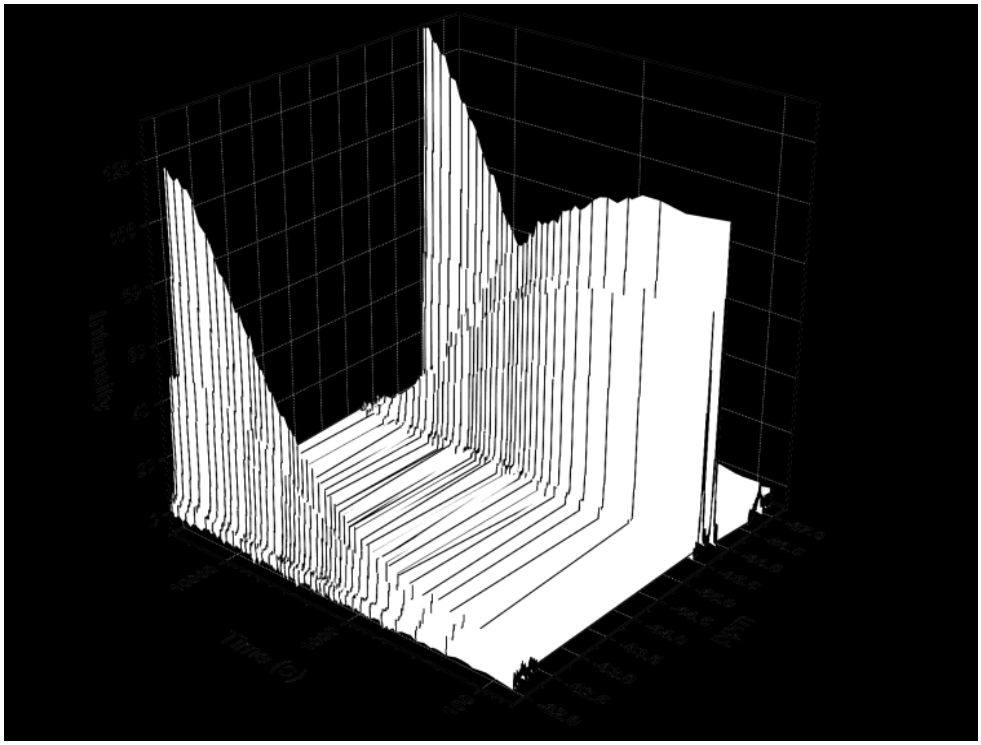

Figure 3. Transient-state nuclear magnetic resonance changes observed for *h*OAT reacting with BCF_3. *h*OAT (333 μM final) was mixed with BCF_3 (247 μM) and ^{19}F spectra (16 scans per spectrum) were collected every 1 min for 8 h. The spectra were culled to approximate a logarithmic time base and were fit simultaneously to a linear A->B model that returned a rate constant of 0.00015 ± 0.00003 s^{-1}.

The transient-state single-turnover NMR spectral data report only on the slow steps of the *h*OAT BCF_3 reaction. The initial spectrum obtained at ~300 sec is assigned as external aldimine II. This state of the reaction has eliminated one fluorine (by integration) as a fluoride that is observed at -120 ppm (**Figure S1**). The elimination of the single fluorine conceivably could occur to yield the E or Z configuration about the exocyclic vinylic bond of external aldimine II. That a

single set of NMR signals is observed at 300 sec indicates that the external aldimine II species is permitted free rotation within the active site (**Figure S2**). These signals resolve to products with two configurations by 480 min, both of which have a predicted mass equivalent to the mass determined for this product(s) in prior studies with BCF_3[8]. While the proportion of E and Z configurations of the turnover products cannot be known by these methods, the structure of the covalently inhibited state indicates that only the E configuration formed by nucleophilic attack by Lys292 is able to bring about irreversible *h*OAT inhibition (**Scheme 2**)[8].

Crystal structure of *h*OAT inhibited by BCF_3: Holoenzyme *h*OAT crystals were obtained in 3 days and had hexagonal prism morphology with the largest dimension of ~ 0.4 mm. The crystals were stable during soaking and diffracted to 1.96 Å resolution. After molecular replacement and refinement, the best refined molecular model had three monomers in an asymmetric unit in the $P3_221$ space group (**Table S1**). The biological assembly of *h*OAT is a typical homodimer which can be reconstructed using the symmetrically related subunit in the crystal lattice (**Figure S3**).

The decay of external aldimine II is exceedingly slow compared to all prior steps observed. For this reason, we attempted to trap this intermediate by soaking. Crystallized *h*OAT was soaked with 1 mM BCF_3 (1 μL added to a 4 μL hanging drop) for 40 min and then frozen in liquid nitrogen. Given that the decay of the external aldimine II intermediate is rate limiting for both BCF_3 inactivation and turnover, the majority fraction of *h*OAT will accumulate as external aldimine II in the presence of excess BCF_3. The active site of the structure of *h*OAT soaked with BCF_3 is shown in (**Figure 4)** and compared with the structure of the covalently inhibited state of *h*OAT determined previously[7] (pathway *b*, **Scheme 2**). The density observed in the active site was interpreted as the external aldimine II intermediate. The electron density supports that PLP has been covalently modified while the conserved Lys292 is detached from the PLP-inactivator adduct. The resolution

of this structural data (1.96 Å) permitted assignment of the five remaining fluorine atoms in this adduct (**Figure S4**). At this stage of the reaction, Lys292 is available for a nucleophilic attack either at the PLP imine carbon or the carbon of a difluoromethylenyl group (pathway *a* and *b* respectively in **Scheme 2**).

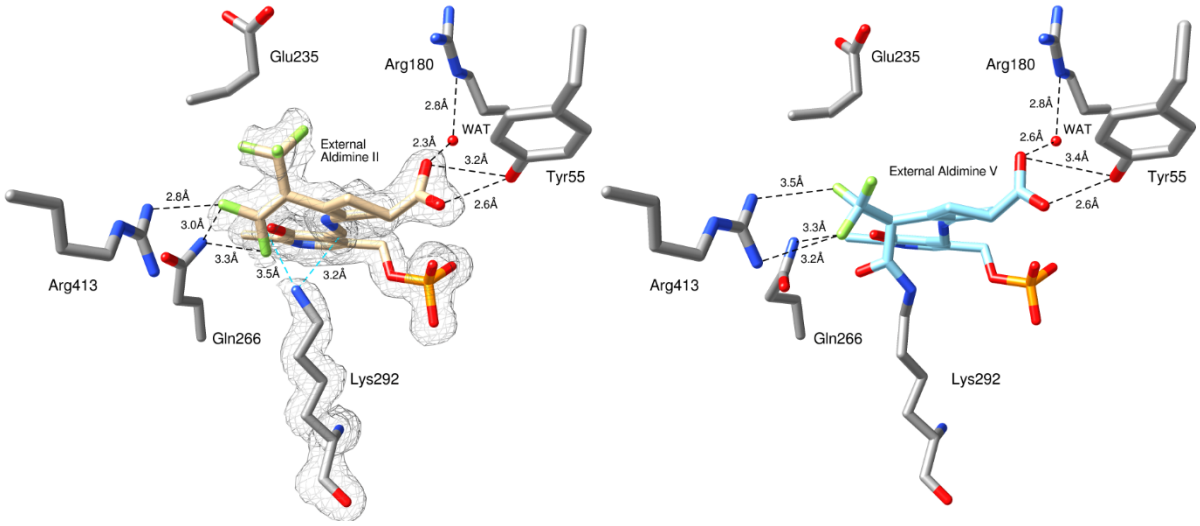

Figure 4. Comparison of the *h*OAT structures of the external aldimine II state and the covalently inhibited complex, external aldimine V. Left: crystal structure of external aldimine II (intermediate, PDB code: 7JX9). The proposed attack distances are shown as dashed lines in cyan and potential hydrogen bonding distances are shown as dashed lines in black. A simulated annealing composite map (2Fo-Fc) at 1.1 σ level is shown in gray color for Lys292 and the external aldimine II intermediate. Right: crystal structure of external aldimine V (final product, PDB code: 6OIA). A water molecule is labeled as WAT.

The external aldimine II intermediate interacts with key residues in the *h*OAT active site (**Figure 4**). The carboxylate group forms apparent hydrogen bonds with Tyr55 whose native function is to bind the α amino group of ornithine[18]. The distance between the carboxylate and the amino group of BCF_3 is shorter than the distance between the ε amino group and the α carboxylate of ornithine. To ensure the formation of external aldimine I, it is required that the carboxylate of BCF_3 be more proximal to PLP than ornithine. As a result, the conserved Arg180, which is proposed to interact

with the α carboxylate group of ornithine, interacts instead with BCF_3 indirectly via an ordered water molecule (**Figures S5** & **4**). The difluoromethylenyl group is observed to interact with Arg413 and Gln266. The native function of Gln266 is to interact with PLP via the pyridyl 5'-hydroxyl group. In the native reaction Arg413 is prevented from interacting with the ornithine carboxylate by a salt bridge with Glu235. In the native OAT reaction this salt bridge can be broken by the dicarboxylic substrates, α-ketoglutarate or glutamate (**Scheme 1**). The trifluoromethyl group of the external aldimine II state is crowded against the aliphatic portion of the Glu235 side chain constraining its conformation away from complementary interaction with the guanidinium of Arg413. In addition to the aliphatic portion of Glu235, two other residues contribute to the binding of external aldimine II via hydrophobic interactions: Phe177 and Tyr85. Collectively, these interactions define an active site cavity that closely contours about the BCF_3 derived moiety, providing specific molecular recognition (**Figure S6**).

The primary difference between the crystal structure of the external aldimine II intermediate, and the final adduct is covalency of the syn-allylic carbon of what was initially the hexafluoropropan-2-ylidine group with Lys292. The structure of this intermediate indicates that the covalent linkage to Lys292 is yet to form. This unliganded lysine and the five remaining fluorine atoms are the defining features of the density that identifies the external aldimine II state. The loss of one fluorine atom from this structure correlates well with the fluoride ion observed to accumulate within the first scans in single turnover monitored by ^{19}F-NMR spectrometry (**Figure S2**). Moreover, the free fluoride ion signal was unchanging throughout subsequent data acquisition, indicating that only one fluorine atom is displaced prior to the reformation of the PLP. The difluoromethylene group in external aldimine II was converted to form the amide bond in aldimine V linked to Lys292. The transition to the covalently inhibited state leaves the remaining

trifluoromethyl group to interact with Arg413 and Gln236. Glu235 remained oriented away from interaction with Arg413 and no longer crowded against the trifluoromethyl group of the inactivator.

Integrating Discussion: Formulating the mechanism for inhibition of *h*OAT by BCF_3 required the use of complementary time-dependent spectroscopic methods. These approaches provide redundancy to the cumulative observations facilitating definitive assignment of the reaction coordinate intermediates. *h*OAT reacts with BCF_3 to form an initial external aldimine species that accumulates in the deadtime of the stopped-flow instrument. The dependence of the decay of this species to the quinonoid provided a means of characterizing the equilibrium that forms the external aldimine species. These data indicate that the dissociation constant of this species is relatively weak (~3 mM), consistent with BCF_3 being a nonnative substrate. Decay of external aldimine I resulted in characteristic spectral transitions associated with a quinonoid species (**Figure 2**, **Scheme 2**). The fit of the formation and decay of this species returned rate constants that indicate ~75% accumulation of a quinonoid at the highest concentrations of BCF_3 with an extinction coefficient for this species at 567 nm of 36,000 $M^{-1}cm^{-1}$. These observations yielded a relatively good kinetic description for the steps that led to the formation of the quinonoid and its ensuing decay. It is the decay of quinonoid I that forms the quasi-stable and key intermediate for *h*OAT inhibition, external aldimine II. Prior characterization of the interaction of BCF_3 with *h*OAT identified that only 8% of any turnover reaction resulted in irreversible inactivation of the enzyme (pathway *b* in **Scheme 2**)[13]. Consequently, BCF_3 is for the majority fraction a substrate for *h*OAT, and only repeated turnovers with fractional partitioning will inactivate the entire enzyme population. Previous studies had also suggested that PLP is hydrolyzed from external aldimine V,

leaving Lys292 covalently modified by BCF_3. The basis for this conclusion was the detection of PLP in inactivated *h*OAT solutions by mass spectrometry[8]. The origin of this PLP is now known to be from the substrate mode of BCF_3, as the final inhibited state of the enzyme was since shown by X-ray crystallographic characterization to be external aldimine V[8].

Different interactions with the active site for the external aldimine II intermediate and the external aldimine V product indicate that the initial binding mode of BCF_3 is significantly different from the orientation of the final product (**Figures 4** & **S5**). The structure reported herein for external aldimine II provides evidence of the initial binding orientation of BCF_3. It is likely that the carboxylate group of BCF_3 interacts with the hydroxyl group of Tyr55 throughout the inactivation reaction. This is the result of a shorter distance between the carboxylate and the amino group in BCF_3 compared to the α-carboxylate and the ε-amino group of ornithine. For the Schiff base formation between BCF_3 and PLP, the carboxylate pivots toward the PLP cofactor, interacting with Tyr55 instead of Arg180, which has been proposed to interact with the α-carboxylate of ornithine (**Figure S5**).[18]

Figure 5. BCF_3 and previously developed mono-trifluoromethyl inhibitors. Top: Structures of the inhibitors. Bottom: Structures of the first intermediates (external aldimines) after initial binding.

In previous studies, two mono-trifluoromethyl derivatives similar to BCF_3 were tested as *h*OAT inhibitors (**Figure 5**).[7,8] The data indicated that the bistrifluoromethyl compound BCF_3 is a better inactivator than either the *syn*- or *anti*-monotrifluoromethyl compounds. Based on the structures reported in this work and previously[8] (**Figure 4**), the role of the bistrifluoromethyl group in improved potency can be attributed to three factors. First, BCF_3 possesses a larger volume that better fills the active site cavity of *h*OAT, confining the chemical possibilities. Second, both trifluoromethyl groups contribute to binding in the initial complex. The *anti*-positioned trifluoromethyl group disrupts a salt bridge between Arg413 and Glu235. Arg413 in turn interacts initially with the *syn*-positioned trifluoromethyl group and the difluoromethylenyl group in the external aldimine II intermediate. Third, elimination of one fluoro group as fluoride, can yield either the E or Z isomer. The E and Z states of external aldimine II both advance on dominant pathway *a* and yield two products that differ only in their configuration about the exocyclic vinylic bond (**Scheme 2**). The structure of the covalently inhibited enzyme indicates that only the E-isomer of external aldimine II can advance to form the covalently inhibited complex. The remaining CF_3 group can reassume the role of interacting with Arg413, thereby contributing to the formation of the final adduct external aldimine V. As a direct consequence of these interactions, BCF_3 displays improved specificity against *h*OAT compared to prior drug candidates with similar structures such as gabaculine, canaline, and FCP.[12,19,20]

The electronegative nature of fluorine atoms has substantial impact on the orientation of BCF_3 during initial binding and during the ensuing chemistry. The fluorine has a propensity to form hydrogen bonds that are weaker than those formed with oxygen or nitrogen atoms.

Consequently, in many cases hydrophobic interactions with fluoro groups can have a significant impact on the stabilization of enzyme-substrate complexes compared to fluorine hydrogen-bonding interactions[21]. Vulpetti et al. hypothesized that relatively shielded fluorine atoms tend to form hydrogen bonds when bound to proteins, while relatively deshielded fluorines prefer hydrophobic interactions[22, 23]. Initially, during inactivation of *h*OAT by BCF_3, the fluorine atoms of both trifluoromethyl groups are deshielded by proximity to the other fluorines. The anti-CF_3 group thus interacts with the aliphatic carbons of the Glu235 sidechain via hydrophobic interactions, breaking the salt bridge between this residue and Arg413. As the reaction proceeds, either the anti- or syn-CF_3 group loses one fluorine atom partially shielding the remaining two fluorines at this site. Therefore, the difluoromethyl group of external aldimine II preferentially forms hydrogen bonds with Arg413 and Gln266. (**Figures 4** & **S6**). This interaction may in turn project weak shielding effects over the distant CF_3 group that would preferentially participate in hydrophobic interactions with Glu235. Conversely, in the external aldimine V state, the local chemical environment of the vicinal CF_3 group has changed. The amide linkage to Lys292 is expected to shield this group so that it prefers to form hydrogen bonds with Arg413 and Gln266.

According to the proposed chemical mechanism the irreversible inactivation of *h*OAT proceeds via a series of chemical oscillations between aldimine and quinonoid states (**Scheme 2**). The nucleophilic attack of Lys292 to the difluoromethylene of external aldimine II tethers only the E-configuration of the inhibitor and each subsequent decay of ensuing quinonoid state yields one fluoride ion. This repeating process ultimately denudes all fluorines from one of the CF_3 groups, solidifying the covalent link to Lys292 and eliminating a path to reinstate an active form of the cofactor. This oscillation terminates with a chemically isolated aldimine, external aldimine V (**Figure 3**). In contrast, in the dominant substrate pathway (pathway *a*) for BCF_3, Lys292 attacks

the carbon of the PLP imine bond of external aldimine II and subsequent hydrolysis results in the regeneration of the active pyridoxal form of the active enzyme. The latter pathway does not regenerate BCF_3 so that multiple turnovers are required to bring about complete inactivation. The decay of aldimine II is slow, resulting in nearly complete fractional accumulation of this species in the steady state, which facilitated capture of this state *in crystallo* (**Figures 4** & **S4**). This structure not only provides direct structural evidence for the proposed inactivation mechanism, but also a foundation for design of molecules that bias the partition of this species toward covalent inhibition. Collapse of the iminium ion of external aldimine II to form quinonoid II would require the Lys292 ε-amino group to be positioned at an angle of ~107° from the plane of the π-system of the difluoromethylenyl group[24]. Although the crystal structure does indicate that the position of the ε-amino group of Lys292 is proximal (3.3 Å, Figure 4), it is in the plane of the difluoromethylenyl group and one of the fluorine atoms partially occludes the electrophilic carbon. While neither pathway is particularly favored by the observed intermediate's position, it is these conformational restrictions that dictate the order of magnitude lower probability for the pathway that inactivates *h*OAT relative to PLP regeneration.

The above analysis serves as a revision of the previously proposed inactivation mechanism of *h*OAT by BCF_3. Within ~20 seconds the interaction of BCF_3 with *h*OAT would result in the accumulation of external aldimine II and inhibit the target enzyme effectively by stabilizing this state. Inactivation via aldimine V would require an excess amount of BCF_3 compared to the enzyme so that multiple turnovers bring about the irreversible inactivation[7]. The rate constants determined for the decay of external aldimine II state can be modelled using numerical integration to show that covalent inactivation requires ~20-fold excess of BCF_3 and then only asymptotically approaches complete inactivation over ~10 days. By itself, this slow rate of inactivation to aldimine

V is unlikely to be effective in suppressing *h*OAT activity *in vivo*, as the high rate of expression in cancer cells is very likely to exceed the rate of covalent inhibition. Therefore, the primary and medically relevant mode of BCF_3 inhibition is trapping the vast majority of *h*OAT as aldimine II, and formation of aldimine V only modestly contributes to the long-term potency of the compound. In regard to iterative rational design, it may be desirable to create the next generation of drug candidates that bias the conversion from external aldimine II to quinonoid II, thereby altering the partition ratio and requiring less inhibitor for complete covalent inactivation. Transient inhibition of *h*OAT using stoichiometric doses of BCF_3 will trap the enzyme as aldimine II and return the majority fraction to an active state within a few days. Therefore, BCF_3 also has the potential to be used as a chemotherapy sensitizer[25] that transiently halts the activity of *h*OAT to increase the susceptibility of cancer cells to other chemotherapeutic agents.

Conclusions: Conventional methods to characterize mechanism-based inhibition involving combinations of mass spectrometry and ligand co-crystallization are effective to both identify the final adduct and to propose overall mechanisms. However, for amenable systems transient kinetic studies are an effective additional method to reveal further mechanistic details. The characteristic intermediate spectra observed for *h*OAT reacting with BCF_3 and the slow kinetics under single turnover conditions provide considerably greater detail of the inactivation mechanism, prompting a revision of BCF_3's potency that is now ascribed to the formation of the external aldimine II species and not the irreversible covalent external aldimine V species as previously described. The accumulation of this quasi-stable intermediate in a short time frame (~20 sec) provides a high steady-state concentration of this species such that crystal soaking could be employed to trap a near homogenous intermediate in the crystal structure during turnover. The crystal structure obtained provides the structural basis for rational design of future inhibitor/inactivator candidates.

We confirm that BCF_3 is a prominent drug candidate that relies on its overall structure for specificity but requires an excess to ensure irreversible inactivation. Such a requirement is a result of a non-ideal attack angle during the conversion from external aldimine II to quinonoid II. However, the slow decay of aldimine II results in essentially all of the enzyme being trapped in this state and thus effectively inhibited soon after administration.

MATERIALS AND METHODS

Materials: All chemicals were purchased from Millipore-Sigma, unless otherwise noted. All enzymes used for cloning were purchased from New England Biolabs.

Expression, and Purification of Human OAT: *h*OAT was expressed and purified according to previously published protocols[12]. See supporting information.

Transient State Methods: The reaction of BCF_3 with *h*OAT was observed in transient state using three approaches. These methods captured signals for both relatively fast and slow chemical transformations. The first three steps in the reaction were captured using a Hitech Scientific (TgK) stopped-flow spectrophotometer in combination with charged coupled device detection (260-800 nm). In these experiments 9.84 μM *h*OAT was allowed to react with 2-fold serially diluted BCF_3 concentrations (63, 127, 254, 508, 1,016, 2,035, 4,065 μM) in 50 mM HEPES, 200 mM NaCl, pH 7.5 at 10 °C (all reported concentrations are after mixing in a 1:1 ratio).

Individual reaction traces at 567 nm for each BCF_3 concentration were extracted from the multiwavelength datasets and combined into a single file. These data were fit globally to the biege portion of the model depicted in (**Scheme 3)** using KinTek Explorer software (KinTek Corp). The CCD spectral datasets for singular value decomposition (SVD) deconvolution were collected at a concentration of BCF_3 equal to 2.08, 4.16 and 8.32 mM. Duplicate shots were acquired using a log time base for two timeframes (0.0025 – 12.4 seconds and 0.0025 – 2,480 seconds). Duplicate datasets for any one timeframe were averaged and spliced together at 12 seconds to form one dataset with sufficient time resolution to accurately describe fast and slow processes. The hybrid dataset was fit globally to the green portion of the model depicted in (**Scheme 3)** using the Spectrafit SVD module of KinTek Explorer software. In this model the rate constant for k_4 was fixed to the value measured using transient state NMR.

^{19}F-NMR spectral observation of the reaction was used both to measure the slowest step observed and to verify the chemistry through spectral assignment of the species that decay and accumulate. A single turnover condition was established by mixing *h*OAT (333 μM) with BCF_3 (247 μM), and ^{19}F-NMR spectra (16 scans per spectrum) were acquired at 1 min intervals for 8 hours (for acquisition parameters, see Supporting Information). The time of the first spectrum equated to ~300 seconds after the reaction commenced and so captures data for the external aldimine II species onward. Spectra were culled to approximate a logarithmic time base and to eliminate intervening portions of the ppm axis that contained no data. The time dependence of these NMR spectra were fit globally to a one-step model that is depicted as the blue portion of (**Scheme 3**).

Crystallization and Crystal soaking of *h*OAT with BCF_3: Purified *h*OAT was buffer exchanged into 50 mM HEPES, pH 7.5 and concentrated to a protein concentration of 6 mg mL^{-1}. The previously reported crystallization conditions[12] were further optimized using the hanging drop vapor diffusion method by varying PEG 6000 (8-12%), NaCl (100-250 mM), and glycerol (0-10%) with a fixed buffer concentration of 100 mM Tricine, pH 7.8. For each hanging drop, either 2 or 3 μL of protein solution was mixed with equal volume of well solution. Several rounds of seeding were applied to improve crystal size and quality. The crystals with the best morphology and size grew in a final condition containing 10% PEG 6000, 100 mM NaCl, and 10% glycerol. BCF_3 (0.5 µL, 1 mM final) was added to the *h*OAT crystal drop and allowed to soak for 40 min. After soaking, crystals were transferred to a cryo-protectant solution (well solution supplemented with 30% glycerol and 1 mM BCF_3) and frozen in liquid nitrogen.

X-ray Diffraction and Data Processing: Monochromatic X-ray diffraction data were collected at the LS-CAT beamline 21-ID-D at the Advanced Photon Source at Argonne National

Laboratory. Data were collected at a wavelength of 1.127 Å and a temperature of 100 K using a Dectris Eiger 9M detector. Data sets were processed and analyzed with autoPROC software[26].

Model Building and Refinement: The *h*OAT structure was solved by molecular replacement using PHASER[27] in Phenix. The starting search model was the previously published structure of *h*OAT (PDB code: 1OAT[28]). The model building and refinement were accomplished in Coot[29] and Phenix[30], respectively, as an iterative process until the lowest possible R_{free}/R factor values were attained. Structural depiction figures were prepared using UCSF Chimera[31].

Accession Code: 7JX9 (PDB code)

Acknowledgement: We thank the generous help from beamline scientists at LS-CAT, especially Dr. Z. Wawrzak, during data collection. This research used resources of the Advanced Photon Source, a U.S. Department of Energy (DOE) Office of Science User Facility operated for the DOE Office of Science by Argonne National Laboratory under Contract No. DE-AC02-06CH11357. Use of the LS-CAT Sector 21 was supported by the Michigan Economic Development Corporation and the Michigan Technology Tri-Corridor (Grant 085P1000817). We also thank our colleague Dr. D. Becker for his willing insights into the *h*OAT inactivation mechanism that permitted a working assignment of the NMR spectra observed during inactivation.

Funding Sources

This research was supported by National Science Foundation Grant CHE-1904514 to D.L. and National Science Foundation Grant 1904480 to G.R.M and National Institutes of Health Grant R01 DA030604 to R.B.S.

References:

[1] Eliot, A. C., and Kirsch, J. F. (2004) Pyridoxal phosphate enzymes: mechanistic, structural, and evolutionary considerations, *Annu Rev Biochem 73*, 383-415.

[2] Mehta, P. K., Hale, T. I., and Christen, P. (1993) Aminotransferases: demonstration of homology and division into evolutionary subgroups, *Eur J Biochem 214*, 549-561.

[3] Hayashi, H. (1995) Pyridoxal enzymes: mechanistic diversity and uniformity, *J. Biochem. 118*, 463-473.

[4] Ginguay, A., Cynober, L., Curis, E., and Nicolis, I. (2017) Ornithine Aminotransferase, an Important Glutamate-Metabolizing Enzyme at the Crossroads of Multiple Metabolic Pathways, *Biology (Basel) 6*.

[5] Wang, G., Shang, L., Burgett, A. W., Harran, P. G., and Wang, X. (2007) Diazonamide toxins reveal an unexpected function for ornithine delta-amino transferase in mitotic cell division, *Proc Natl Acad Sci U S A 104*, 2068-2073.

[6] Lee, H., Juncosa, J. I., and Silverman, R. B. (2015) Ornithine aminotransferase versus GABA aminotransferase: implications for the design of new anticancer drugs, *Med Res Rev 35*, 286-305.

[7] Zigmond, E., Ben Ya'acov, A., Lee, H., Lichtenstein, Y., Shalev, Z., Smith, Y., Zolotarov, L., Ziv, E., Kalman, R., Le, H. V., Lu, H., Silverman, R. B., and Ilan, Y. (2015) Suppression of Hepatocellular Carcinoma by Inhibition of Overexpressed Ornithine Aminotransferase, *ACS Med Chem Lett 6*, 840-844.

[8] Moschitto, M. J., Doubleday, P. F., Catlin, D. S., Kelleher, N. L., Liu, D., and Silverman, R. B. (2019) Mechanism of Inactivation of Ornithine Aminotransferase by (1S,3S)-3-Amino-4-(hexafluoropropan-2-ylidenyl)cyclopentane-1-carboxylic Acid, *J Am Chem Soc 141*, 10711-10721.

[9] Abeles, R. H., and Maycock, A. L. (1976) Suicide Enzyme Inactivators, *Acc. Chem. Res. 9*, 313-319.

[10] Juncosa, J. I., Takaya, K., Le, H. V., Moschitto, M. J., Weerawarna, P. M., Mascarenhas, R., Liu, D., Dewey, S. L., and Silverman, R. B. (2018) Design and Mechanism of (S)-3-Amino-4-(difluoromethylenyl)cyclopent-1-ene-1-carboxylic Acid, a Highly Potent gamma-Aminobutyric Acid Aminotransferase Inactivator for the Treatment of Addiction, *J Am Chem Soc*.

[11] Le, H. V., Hawker, D. D., Wu, R., Doud, E., Widom, J., Sanishvili, R., Liu, D., Kelleher, N. L., and Silverman, R. B. (2015) Design and Mechanism of Tetrahydrothiophene-Based gamma-Aminobutyric Acid Aminotransferase Inactivators, *J Am Chem Soc 137*, 4525-4533.

[12] Mascarenhas, R., Le, H. V., Clevenger, K. D., Lehrer, H. J., Ringe, D., Kelleher, N. L., Silverman, R. B., and Liu, D. (2017) Selective Targeting by a Mechanism-Based Inactivator against Pyridoxal 5'-Phosphate-Dependent Enzymes: Mechanisms of Inactivation and Alternative Turnover, *Biochemistry 56*, 4951-4961.

[13] Moschitto, M. J., Doubleday, P. F., Catlin, D. S., Kelleher, N. L., Liu, D., and Silverman, R. B. (2019) Mechanism of Inactivation of Ornithine Aminotransferase by (1 S,3 S)-3-Amino-4-(hexafluoropropan-2-ylidenyl)cyclopentane-1-carboxylic Acid, *J Am Chem Soc*.

[14] Zhu, W., Doubleday, P. F., Catlin, D. S., Weerawarna, P. M., Butrin, A., Shen, S., Wawrzak, Z., Kelleher, N. L., Liu, D., and Silverman, R. B. (2020) A Remarkable Difference That One Fluorine Atom

Confers on the Mechanisms of Inactivation of Human Ornithine Aminotransferase by Two Cyclohexene Analogues of gamma-Aminobutyric Acid, *J Am Chem Soc 142*, 4892-4903.

[15] Toney, M. D. (2005) Reaction specificity in pyridoxal phosphate enzymes, *Arch. Biochem. Biophys. 433*, 279-287.

[16] Hayashi, H., and Kagamiyama, H. (1997) Transient-state kinetics of the reaction of aspartate aminotransferase with aspartate at low pH reveals dual routes in the enzyme-substrate association process, *Biochemistry 36*.

[17] Williams, J. A., Bridge, G., Fowler, L. J., and John, R. A. (1982) The reaction of ornithine aminotransferase with ornithine, *Biochem J 201*, 221-225.

[18] Storici, P., Capitani, G., Muller, R., Schirmer, T., and Jansonius, J. N. (1999) Crystal structure of human ornithine aminotransferase complexed with the highly specific and potent inhibitor 5-fluoromethylornithine, *J Mol Biol 285*, 297-309.

[19] Shah, S. A., Shen, B. W., and Brunger, A. T. (1997) Human ornithine aminotransferase complexed with L-canaline and gabaculine: structural basis for substrate recognition, *Structure 5*, 1067-1075.

[20] Storici, P., Qiu, J., Schirmer, T., and Silverman, R. B. (2004) Mechanistic crystallography. Mechanism of inactivation of gamma-aminobutyric acid aminotransferase by (1R,3S,4S)-3-amino-4-fluorocyclopentane-1-carboxylic acid as elucidated by crystallography, *Biochemistry 43*, 14057-14063.

[21] Reddy, V. P. (2015) *Organofluorine Compounds in Biology and Medicine*, Elsevier.

[22] Vulpetti, A., and Dalvit, C. (2012) Fluorine local environment: from screening to drug design, *Drug Discov Today 17*, 890-897.

[23] Dalvit, C., Ko, S. Y., and Vulpetti, A. (2013) Application of the rule of shielding in the design of novel fluorinated structural motifs and peptidomimetics, *Journal of Fluorine Chemistry 152*, 129-135.

[24] Burgi, H. B., Dunitz, J. D., Lehn, J. M., and Wipff, G. (1974) Stereochemistry of Raction Paths at Carbonyl Centers, *Tetrahedron 30*, 1563-1572.

[25] Koch, C. J., Parliament, M. B., Brown, M., and Urtasun, R. C. (2010) Chemical Modifiers of Radiation Response, In *Leibel and Phillips Textbook of Radiation Oncology* 3rd ed., pp 55-68, ElsevierHealth.

[26] Vonrhein, C., Flensburg, C., Keller, P., Sharff, A., Smart, O., Paciorek, W., Womack, T., and Bricogne, G. (2011) Data processing and analysis with the autoPROC toolbox, *Acta Crystallogr D Biol Crystallogr 67*, 293-302.

[27] McCoy, A. J., Grosse-Kunstleve, R. W., Adams, P. D., Winn, M. D., Storoni, L. C., and Read, R. J. (2007) Phaser crystallographic software, *J Appl Crystallogr 40*, 658-674.

[28] Shen, B. W., Hennig, M., Hohenester, E., Jansonius, J. N., and Schirmer, T. (1998) Crystal structure of human recombinant ornithine aminotransferase, *J Mol Biol 277*, 81-102.

[29] Emsley, P., Lohkamp, B., Scott, W. G., and Cowtan, K. (2010) Features and development of Coot, *Acta Crystallogr D Biol Crystallogr 66*, 486-501.

[30] Liebschner, D., Afonine, P. V., Baker, M. L., Bunkoczi, G., Chen, V. B., Croll, T. I., Hintze, B., Hung, L. W., Jain, S., McCoy, A. J., Moriarty, N. W., Oeffner, R. D., Poon, B. K., Prisant, M. G., Read, R. J., Richardson, J. S., Richardson, D. C., Sammito, M. D., Sobolev, O. V., Stockwell, D. H., Terwilliger, T. C., Urzhumtsev, A. G., Videau, L. L., Williams, C. J., and Adams, P. D. (2019) Macromolecular structure determination using X-rays, neutrons and electrons: recent developments in Phenix, *Acta Crystallogr D Struct Biol 75*, 861-877.

[31] Paettersen, E., Goddard, T., Huang, C., Couch, G., Greenblatt, D., Meng, E., and Ferrin, T. (2004) UCSF Chimera--a visualization system for exploratory research and analysis, *J Comput Chem 25*, 1605-1612.

Table of Contents Figure: